

DISPERSION MODELLING OF THE KILAUEA PLUME

ANNETTE T. HOLLINGSHEAD¹, STEVEN BUSINGER^{2,*}, ROLAND DRAXLER³,
JOHN PORTER¹ and DUANE STEVENS¹

¹University of Hawaii, Honolulu, HI 96822, U.S.A.; ²Department of Meteorology, 2525 Correa Rd. Honolulu, HI 96822, U.S.A.; ³NOAA Air Resources Laboratory, Silver Springs, MD 20910, U.S.A.

(Received in final form 26 August 2002)

Abstract. Emissions from the Kilauea volcano pose significant environmental and health risks to the Hawaiian community. This paper describes progress toward simulating the concentration and dispersion of plumes of volcanic aerosol after they emanate from the Pu'u O'o vent of the Kilauea volcano.

In order to produce an accurate regional forecast of the concentration and dispersion of volcanic aerosol, the Hybrid Single-Particle Lagrangian Integrated Trajectory (HY-SPLIT) model was used. Wind fields and thermodynamic data from the non-hydrostatic Mesoscale Spectral Model (MSM) were employed as input for the HY-SPLIT model. A combination of satellite remote sensing, aircraft, and ground-based observations collected during a field experiment was used to validate the model simulation of aerosol distribution.

The HY-SPLIT model shows skill in reproducing the plume shape, orientation, and concentration gradients as deduced from satellite images of aerosol optical depth. Comparison of the modelled and observed values suggests that the model was able to produce reasonable plume concentrations and spatial gradients downwind of the source. Model concentrations were generally less than those observed on the leeward side of the Island of Hawaii. This deficiency may be explained by a lack of (i) background concentrations, (ii) local sources of pollution and/or (iii) sea-breeze circulation in the prognostic input wind field. These results represent early progress toward the goal of future operational application of the HY-SPLIT model to predict volcanic aerosol concentrations in Hawaii. This may help mitigate their negative impacts of plumes respiratory health, agriculture, and general aviation.

Keywords: HY-SPLIT, Kilauea volcano, Regional spectral model, Sulfate aerosol.

1. Introduction

The Kilauea volcano on the Island of Hawaii is the longest actively erupting volcano in the world. The most recent eruptive phase began in January 1983 and the first four years of the eruption included sensational episodes of lava fountains. Sulfur dioxide (SO₂) emissions from Kilauea's East Rift Zone have ranged from 1,000 to 7,000 tonnes of SO₂ per day during 1992–1998 and up to 32,000 tonnes per day during the past 13 years (Elias et al., 1998). Under weather patterns that produce southerly winds,** SO₂ is advected over the town of Volcano located approximately 10 km to the north-west of the vent. A stationary correlating spec-

* Corresponding author, E-mail: businger@soest.hawaii.edu

** Southerly winds are also known as kona winds in Hawaii.



trometer (COSPEC) monitor located in Volcano has measured minute-averaged SO₂ concentrations up to 1300 ppb and on average exceeding 290 ppb in a single day (Elias, 1992; Sutton and Elias, 1993, 1996, 1997).^{*} These observations far exceed the Environmental Protection Agency's accepted health standard of 145 ppb of ambient SO₂ over a 24-hour period.

Kilauea's emissions go through several chemical transformations after they enter the marine boundary layer (MBL). SO₂ rapidly undergoes gas to particle conversion in the presence of high relative humidity, characteristic of the vent emission (Morrow, 1991). The resulting sulfate aerosol is hygroscopic and remains in solution at ambient relative humidities. The hygroscopic nature allows the aerosol to expand up to three times its original volume (Porter and Clarke, 1997). At 70% relative humidity, typical of Hawaiian trade wind conditions, sulfate aerosol is about 30% sulfuric acid and ~70% water (Palmer and Williams, 1975).

The small particle sizes that characterize the sulfuric acid aerosol have very slow settling velocities, and thus the aerosol accumulates in the boundary layer under light wind conditions. It is these particulates that most strongly impact visibility, resulting in a plume of nearly opaque volcanic smog, also known as *vog*. During episodes of increased sulfate production and atmospheric stagnation, the *vog* aerosol concentration may become large enough, particularly near the tradewind inversion, to create a significant visibility hazard for general aviation (Figure 1).

The small size-distribution of the sulfate particulates allows them to effectively reach down into the human lung. In the presence of high relative humidity in the human body, the hygroscopic aerosol readily expands to maximum volume, irritating and obstructing airways. In addition to lung irritation, the presence of *vog* has been linked to asthma, sinusitis, respiratory disease, lung cancer and/or chronic obstructive pulmonary disease (Kleinman, 1995; Ruben et al., 1995; Mannino et al., 1995; Worth, 1995).

Parts of the Hawaiian Islands are at an elevation (e.g., near the height of the tradewind inversion) and downwind location such that the *vog* plume regularly intersects them (e.g., Figure 1). Consequently, these areas are frequently subject to the full corrosive impact of the sulfuric acid aerosol. Moreover, rain falling from clouds that form in the *vog* plume can also be highly acidic. The resulting acid condition negatively impacts agriculture and leaches lead from metal roofs and plumbing (State of Hawaii, Department of Health, 1989).

In summary, *vog* poses a significant environmental and health risk to the Hawaiian community and the potential benefit of monitoring the *vog* plume and providing forecast guidance is evident. The primary goal of this research is to create a prognostic tool to aid in the prediction of *vog* plume dispersion. Simulation results were validated using aerosol concentrations derived from aircraft measurements, ground-based data, and satellite imagery.

^{*} These data are sampled every second, averaged every minute, and stored hourly courtesy of National Park Service, Air Resources Div., and USGS, Hawaiian Volcano Observatory.

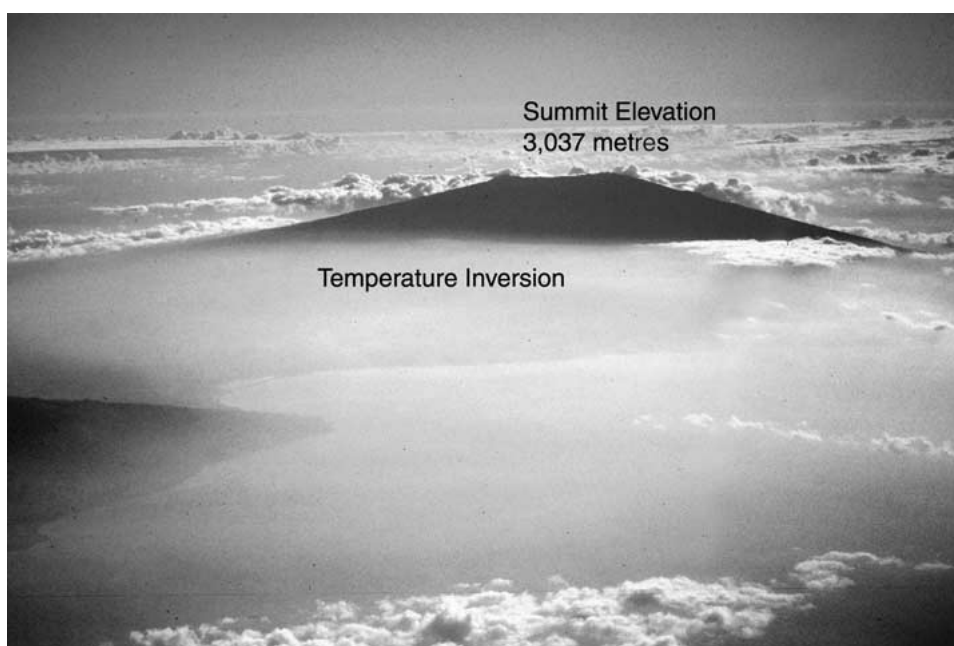


Figure 1. Aerial photograph of Maui showing the lower slopes of Haleakala obscured by vog on 25 January 2000. Photograph taken from the west by Annette Hollingshead.

1.1. BACKGROUND

Kilauea has remained in a more quiescent outgassing stage during the past 14 years. From February 1992 to the present the Pu'u O'o vent has been the most active of the Kilauea vents (Harris and Thornber, 1999). Located on the east rift zone (Figure 2), it is responsible for up to 70% of the total SO₂ emission (Realmuto et al., 1997). The Kilauea Volcano is unique in that it is considered sulfur rich in contrast to other volcanoes. Comparisons of gas samples from numerous volcanic sources show that volcanoes composed of dacite or andesite magma (i.e., Mount St. Helens and Mount St. Augustine, respectively) contain considerably less SO₂ than basalt-type volcanoes like Kilauea, up to six orders of magnitude less in mole percentages (Gerlach and Casadevall, 1986; Gerlach, 1993; Symonds et al., 1994). The Pu'u O'o vent is the first atmospheric window that lava encounters as it flows toward the surface. The vent is cone-shaped, consisting of a 1-km diameter opening at the surface, which narrows to 300 m at the base of the chasm. A significant pressure difference exists between the lava approaching the skylight and the surface of the Pu'u O'o vent. The lava passing beneath the vent, but remaining below the surface, experiences a rapid decrease in pressure and consequently large amounts of volcanic gas are emitted to the environment through the vent. In this way this large vent acts as a pseudo-chimney. Kilauea's vent structure has changed significantly over the past 18 years. During certain episodes, the Kupa'ianaha vent provided the

primary outlet for lava. During other periods, the tube systems flowed freely and drained much of the lava from the Pu'u O'o and Kupa'ianaha lava ponds, decreasing the emission rates at the vents. Lava outgassing continues past the lava ponds on its path below the surface where it flows through numerous tube systems. Gases escape through ceiling breaks in the tubes and as lava approaches the coastline. However, by the time outgassing occurs along the tube system, a large depletion in primary gases, including sulfur dioxide, has already occurred. Since it is currently the dominant source of SO₂ release, outgassing from the Pu'u O'o vent will be the focus of the modelling of this research.

The volcanic aerosol plume is composed mainly of water vapour, SO₂, and sulfate particulates. As mentioned previously, SO₂ rapidly converts to sulfate particulates in the high relative humidity conditions near the main vent. This observation is confirmed by measurements taken at the Department of Health (DOH) monitoring station located in Captain Cook (see Figure 2a for location). The DOH continuous pulsed fluorescent ambient air analyzer detects only trace amounts of SO₂, yet high amounts of particulate matter are measured (PM₁₀ particulates <10 μm in diameter). The formation of sulfuric acid can occur as new particle formation (homogeneous nucleation) or as the addition of mass to existing aerosols (Pruppacher and Klett, 1978). In clean conditions, existing particle numbers are low, leading to new particle formation. Homogeneous nucleation also occurs more easily in areas of high SO₂ content, such as in the volcano plume. Within hours of their formation, these new particles coagulate to a stable size distribution (the accumulation mode) (Hoppel et al., 1987). The accumulation mode ranges from 0.1–0.6 μm diameter and has been found to be quite stable (Pruppacher and Klett, 1978; Porter and Clarke, 1997). Once sulfuric acid aerosols are formed, the addition of naturally existing ammonia can partially neutralize the aerosol to form ammonium bisulfate, (NH₄)HSO₄, or totally neutralize the aerosol to form ammonium sulfate, (NH₄)₂SO₄. However, volatility measurements in the volcano plume show that the aerosols remain highly acidic, with very little neutralization even after being advected more than 1,600 km downwind (Clarke and Porter, 1991).

Vog dispersion is primarily a function of synoptic and local wind patterns as well as environment stability. The majority of the vog pollutants are trapped within the subtropical boundary layer in the vicinity of Hawaii by a strong prevailing inversion (Figure 1). The inversion is the result of a persistent North Pacific high-pressure system centered just north-east of the Hawaiian Islands, which is also responsible for prevailing north-east trade winds that characterize Hawaii's weather. The prevailing trade winds advect the vog pollutants from their source towards the south-west. Island blocking of the trade wind flow produces a clockwise eddy to the west of South Point, which advects the vog along the leeward coast (Figure 2a). Vog is advected onshore during the afternoon hours when solar heating of the land surface along with light winds on the leeward coast result in a strong localized sea-breeze circulation. Therefore, vog concentrations are enhanced along the Kona Coast of the Island of Hawaii during prevailing tradewind conditions.

Weak inversions, strong trade winds, and southerly winds (associated with fronts, shear-lines, or kona lows) all act to reduce vog concentrations along the Kona Coast. Gravitational settling of accumulated sulfate aerosols ($<0.24 \mu\text{m}$) is quite small, $<3.5 \text{ mm per second}$ over smooth ocean surfaces (Zhang et al., 2001). As plume elevation increases, gravitation settling becomes negligible as a removal process (Draxler et al., 1994). Generally, gravitational settling becomes significant as a removal process for aerosol greater than $3.8 \mu\text{m}$ over rough terrain (Zhang et al., 2001). Wet removal represents a more viable deposition mechanism for the vog aerosol. The majority of Hawaii's annual rainfall (up to 6000 mm yr^{-1}) occurs on the windward side because of orographic effects upwind of the vent. South Point and inland Kona areas have relatively less precipitation ($500\text{--}2000 \text{ mm yr}^{-1}$) (Giambelluca et al., 1986). The maximum rainfall along the Kona Coast generally occurs with afternoon showers over upland areas associated with the diurnal sea-breeze circulation. Elevated aerosol concentrations along the Kona Coast decrease rainfall efficiency and increase cloud and rain acidity, conditions that appear to adversely impact agricultural crops such as coffee and tropical fruit.

2. Data and Methods

A field experiment was conducted on the Island of Hawaii on 25 and 26 January 2000 (hereafter referred to as *day one* and *day two*, respectively) to document the distribution of the vog aerosol and to provide validation for the modelling effort. During this experiment, aircraft data, ground-based data, and satellite data were collected.

Aircraft data were collected on day one from a Seneca airplane. The plane was equipped with a Microtops II Sun Photometer and GPS to log aircraft position (Morys et al., 1996; Porter et al., 2001). The aircraft sun-photometer measures aerosol optical depth. In order to compare these data with model results, a data conversion from optical depth to dry mass ($\mu\text{g m}^{-3}$) is necessary. Aerosol optical depth (τ) can be expressed

$$\tau = \int_{\text{SFC}}^z \sigma_s \partial z = \bar{\sigma}_s \Delta z, \quad (1)$$

where σ_s represents the column averaged aerosol scattering coefficient (m^{-1}) and Δz designates the depth of the optical layer (Kidder and Vonder Haar, 1995; Charlson et al., 1991). The depth of the boundary layer is a reasonable assumption for Δz since the majority of aerosol remains trapped below the trade wind inversion (e.g., Figure 1). The inversion layer depth was estimated to be 2000 m by interpolating National Weather Service (NWS) radiosonde data from Lihue and Hilo to the flight path. Equation (1) can be rewritten

$$\bar{\sigma}_s = \frac{\tau}{\Delta z}. \quad (2)$$

As an example, the first aircraft-based sun photometer measurement of optical depth at the 500-nm wavelength was 0.072 (no units) resulting in an average column scattering coefficient, $\overline{\sigma_s} = 3.6 \times 10^{-5} \text{ m}^{-1}$. Sulfate aerosol size distribution is dependent upon sulfate species and ambient relative humidity. Based on Mie theory calculations and the size distribution models (Porter and Clarke, 1997), sulfate mass scattering coefficients (σ_{sm}) of $7\text{--}10.5 \times 10^{-3} \text{ m}^2 \text{ kg}^{-1}$ were obtained assuming relative humidities of 65–80% and sulfate aerosol mass values of $2.21\text{--}17.39 \times 10^{-3} \text{ kg}$. These values were chosen to cover the range of conditions expected in the volcanic plume. Note an average mass scattering coefficient of $8 \times 10^3 \text{ m}^2 \text{ kg}^{-1}$ (70% relative humidity) was used as a best value for the calculations in this study. Therefore, the column-averaged sulfate concentration (\bar{C}), in units $\mu\text{g m}^{-3}$, is

$$\bar{C} = \frac{\overline{\sigma_s}}{\sigma_{\text{sm}}}. \quad (3)$$

Using Equations (2) and (3), the first sun photometer measurement results in a column average concentration of $4.5 \mu\text{g m}^{-3}$.

Sulfate aerosol scatter more efficiently than sea-salt aerosol; however, in clean marine boundary conditions, salt particulates are the dominant aerosol (Porter and Clarke, 1997). This introduces a small uncertainty in the above calculations. In the windward and South Point areas, where ocean white-capping is more prominent, this may add a background component to any sun photometer measurements. During the field experiment, measured sun photometer values upwind of the source (excluding waypoint 2 which will be discussed further in the *Results* section) were less than $2.45 \mu\text{g m}^{-3}$. These are most likely representative of background sea-salt aerosol intrusion and were within the error range portrayed in the graphs to follow.

The ground-based data consist of sun photometer measurements observed during day two, using a Microtops II Sun Photometer. Mobile surface measurements were taken during daylight hours with north to south transects along coastal regions while driving along the road. Attention was paid to sky condition to assure that clouds did not obscure the instrument's view of the sun.

Satellite data in this experiment were used to document the shape, size, and location of the vog plume. The satellite data used in this research were obtained by the Sea-viewing Wide Field-of-view Sensor (SeaWiFS), which is mounted on a low Earth orbiting satellite (approximately 278 km above the surface). Satellite measured radiances over the ocean consist of ocean surface radiance (10–20%) and atmospheric radiance (80–90%). In deriving ocean color products, the main charge of the SeaWiFS project, a correction is needed to remove the satellite measured atmospheric radiance. This is accomplished by deriving the aerosol optical concentration and type at near IR wavelengths (760 and 870 nm), where the ocean is nearly opaque, and extrapolating to obtain aerosol radiances at the shorter wavelengths (Gordon, 1997). As a byproduct of this effort, the aerosol optical depth (at 870 nm) can also be obtained from the SeaWiFS algorithm.

3. Model Description

The dispersion model used in this study is the Hybrid Single Particle Lagrangian Integrated Trajectory (HY-SPLIT) and dispersion model (Draxler and Hess, 1997, 1998). HY-SPLIT requires as input high-resolution wind fields and thermodynamic data output from a mesoscale numerical weather prediction (NWP) model. For this purpose output from the non-hydrostatic Mesoscale Spectral Model (MSM) (Juang, 1992, 2000; Juang and Kanamitsu, 1994; Juang et al., 1997) was used.

Global Spectral Model (GSM) data from the National Centers for Environmental Prediction's hydrostatic model are used as input and boundary conditions for a non-hydrostatic high-resolution regional model. This regional model, known as the MSM, is run regularly over a domain that encompasses the Hawaiian archipelago at a spatial resolution of 10 km for a 48-hr forecast period. A 4-km nested grid over the Island of Hawaii provides higher resolution output for this experiment. The Hawaii MSM is run with twenty-second time increments using 26 sigma levels, with numerical data output hourly. Available GSM model data for this experiment included 24-hr forecast runs initialized at 0000 UTC on 23 January through 0000 UTC 28 January 2000. These data were used as initial conditions for the 10-km MSM. Similarly, the 10-km MSM data were used as the initial condition for the 4-km MSM grid. After 24 hours, the next GSM initial conditions were introduced while maintaining any mesoscale perturbations calculated internally on the nested grids on the 24th hr. During the post-processing, data on sigma levels were interpolated to 20 pressure levels. Due to available data output processes at the time, data were output every 100 hPa (e.g., 1000 hPa, 900 hPa, 800 hPa, etc).*

Since the presence of the trade wind inversion is a key component to aerosol dispersion, the vertical temperature gradient must be accurately resolved in the HY-SPLIT model for it to reasonably simulate plume evolution and aerosol concentrations. The temperature gradient occurs over a small vertical extent. Typically the inversion base lies between 2050–2350 m (roughly between 810–770 hPa) during light to moderate trade wind conditions with a mean thickness of 340–379 m (Grinding, 1992). Because of a lack of vertical resolution in the post-processed MSM thermodynamic data, the actual inversion height and strength were estimated and introduced along with the model output winds. To accomplish this, radiosonde data from the Hilo and Lihue soundings were interpolated for each synoptic time (0000 and 1200 UTC) during the field experiment. The model wind data was then re-interpolated to 20 hPa layers and the resulting average radiosonde temperature and relative humidity discontinuities at the inversion were interpolated to the nearest model pressure level. The height and strength of the inferred inversions were maintained until the next available sounding.

Another deficiency in the MSM model output is its inability to correctly simulate the strength of the diurnal circulation in the observed wind field. Both the

* Further detail regarding the MSM design, specifications and current projects can be found at <http://www.mhpc.edu/projects/wswx>

diurnal sea breeze that forms during the day and downslope katabatic winds that form at night are poorly represented in the model output. Repercussions of this deficiency on the position of the simulated vog plume and advection of vog onto the Kona Coast will be discussed in the following sections.

The HY-SPLIT model is a transport and dispersion model (Draxler and Hess, 1998). The trajectory simulations require wind fields on pressure or sigma surfaces and surface pressure as input in order to perform time-integrated advection. In addition, the concentration and dispersion components of the model require moisture and temperature variables to compute the vertical diffusivity profile. Wind shear and horizontal deformation of the wind field are used to compute mixing.

The model disperses pollutants in two ways, by particle or puff method. The particle method releases a discrete number of particulates at onset based upon emission characteristics and the density of aerosols. Each of these particulates is advected along a mean trajectory with a turbulent component added in order to represent the dispersive nature of the atmosphere.

Using the puff method, a single puff is released from the source. This puff starts with a Gaussian distribution based upon initial emission characteristics and is advected using the center point as a single trajectory, thus reducing the quantity of particles necessary for adequate spatial coverage. The Gaussian distribution from each puff at a single concentration increment (Δc) is governed by

$$\Delta c = m(2\pi\sigma_h^2\Delta z)^{-1} \exp\left(\frac{-0.5x^2}{\sigma_h^2}\right), \quad (4)$$

where m is pollutant mass, σ_s is a function of puff radius (r),

$$r = 3.0\sigma_h, \quad (5)$$

Δz is the grid cell height and x is the distance from the puff centre point to the grid-node (Draxler and Hess, 1998). The dispersion is modelled by the puff growth (again adding a turbulent component) along the trajectory; the advantage of this approach is less computation.

The reliability of the particle method tends to deteriorate with larger scale computations because particles achieve wider scatter along the mean trajectory with distance, and calculating the concentration gradient becomes less accurate with increasing distance. Conversely, this method responds more accurately to conditions of strong wind shear (Draxler and Hess, 1997, 1998; Hurley, 1994). However, since this approach becomes computationally taxing, a combination of both methods, horizontal puff advection and vertical particle advection, may be used in order to gain computer efficiency, while retaining the integrity of the model physics. This method is referred to as the part-puff method (Hurley, 1994). Both methods were employed in this research.

The HY-SPLIT model also performs wet and dry deposition calculations. Various depositions are available for both particles and gasses. Since rainfall was not

observed during the field experiment, only dry deposition was included in this research. Dry deposition calculations may be performed implicitly, explicitly or by using gravitational settling. The model calculates dry deposition (D_{dry}) as

$$D_{\text{dry}} = m\{1 - \exp[-\Delta t(V_d \Delta Z_p^{-1})]\}, \quad (6)$$

where m is mass, Δt is the time increment, V_d is the explicit deposition velocity, ΔZ_p represents the depth of the pollutant layer (the lowest model layer). Gravitational settling and implicit methods require additional input parameters to describe particulate composition, in which case the model calculates V_d . Dry deposition was performed explicitly in this research, using 1 mm s^{-1} estimated fall velocities for sulfate (Zhang et al., 2001).*

The MSM output for 0000 UTC on 23 January until 0000 UTC on 28 January 2000 was used as input for the HY-SPLIT model runs. Since there remains much uncertainty regarding the SO_2 to sulfate aerosol conversion rate, the assumption was made that all gas was immediately converted to aerosol near the source, significantly reducing computation time. This is a reasonable assumption given that by the time a parcel journeys from the source to the Kona coast (12–24 hrs depending on parcel height and wind speed), low amounts of SO_2 gas and high concentrations of particulate matter are observed. The emission rate was based on HVO COSPEC estimated SO_2 emissions of $\sim 1,500$ tonnes per day (Elias et al., 1998 and personal communication January 2000). Using a 100% per hr conversion rate of SO_2 to sulfate aerosol yielded a net of 5.67×10^{10} kg of sulfate per hour.

The 3-D particle method was the optimal way to run HY-SPLIT at the high resolution needed over complex island terrain. However, due to the discrete amount of particles released in this mode and lack of pre-existing aerosol, quantitative comparisons at particular locations and times proved difficult. Often the model locations revealed a zero concentration. Therefore, all quantitative concentration comparisons used model values attained through the part-puff method as well as the 3-D particle method. In this case, the Gaussian distribution exhibited the more robust solution.

Model output was produced specifically for the locations of each of the waypoint measurement sites to compare observational and model data. Waypoint locations were determined via a hand held Global Positioning System (GPS).

4. Meteorological Conditions during the Field Experiment

Nearly optimal synoptic conditions were present during the field experiment during day one and day two. These conditions include subsidence associated with a surface high-pressure system in close proximity to the Hawaiian Islands and a relative

* Further detail regarding the HY-SPLIT design and specifications can be referenced at <http://www.arl.noaa.gov/hysplit/>

absence of obscuring high clouds (Figure 3). The subsidence maintains a trade wind inversion that prevents vertical mixing of the vog above the boundary layer. The close proximity of the high-pressure system north-east of Hawaii reduced the north-easterly wind speeds, while still advecting the pollution from the source towards the leeward side of the island. Light winds during the field experiment promoted local aerosol accumulation.

Sea-level pressure (SLP) analyses, available every six hrs from the National Weather Service (NWS), were used to document the synoptic conditions during the field experiment, which changed slowly during this period (Figure 3). At the start of aircraft-based measurements, 1400 HST (0000 UTC) on day one, a 1022-hPa high-pressure system centered to the north-east of Hawaii resulted in light north-easterly winds in the vicinity of the Island of Hawaii (Figure 3a). A second high-pressure centre is located to the north-north-west, with a weak shear line between the two highs. The shear line is associated with a low-pressure system located to the north-east, which gradually moved north-eastward through the period. Winds along the southern side of the islands switched from north-east to south-east just prior to passage of the shear line, which first crossed Kauai and continued eastward towards Hawaii during the next 24 hrs. By 0000 UTC (1400 HST) on day two, the trailing surface high strengthens to 1030 hPa and becomes the dominant system for Hawaii (Figure 3b). North-easterly winds began to strengthen over Kauai as the high pressure neared the state. However, even with moderate ($5\text{--}10\text{ m s}^{-1}$) north-easterly winds over the open ocean north of the Island of Hawaii, light wind conditions persisted over South Point because of a continued weak pressure gradient over the area. The leeward side of Hawaii experienced weak orographically induced southerly flow and a well-defined afternoon sea-breeze circulation near the lee coast. At this time (1400 HST on day two) ground-based measurements proceeded under favorable conditions for advecting vog across the Kona Coast.

National Weather Service sounding data from Lihue, Kauai and Hilo, Hawaii were used to examine atmospheric stability and winds (Figure 4). The Lihue sounding at 1200 UTC on the 25 January shows a $5\text{ }^{\circ}\text{C}$ trade wind inversion of 1838 m (817 hPa) at the western end of the island chain (Figure 4a). Low-level winds were from the west, indicating nocturnal drainage flow emanating from Wai'aleale and Kawaikini summits (elevation 1.6 km). In Hilo, a $3\text{ }^{\circ}\text{C}$ inversion was observed at 1810 m (820 hPa) (Figure 4b), and low-level winds were from the south-west. Because of the orographic impact of the Mauna Loa and Mauna Kea volcanoes (elevation >4 km) near Hilo, low-level winds acquired by the Hilo radiosonde are generally unrepresentative of synoptic conditions upstream of the island. At this time, the low-level south-westerly flow is consistent with a nocturnal drainage flow emanating from Mauna Kea (Feng and Chen, 1998).

Sounding data for 0000 UTC (1400 HST) on day two show that the Lihue inversion strength decreased from $5\text{ }^{\circ}\text{C}$ to $3\text{ }^{\circ}\text{C}$ and the inversion base decreased from 1838 to 1680 m (837 hPa), with low-level winds from the north-east (Figure 4a). The weak shear line passed over Kauai about 4 hrs prior to the sounding

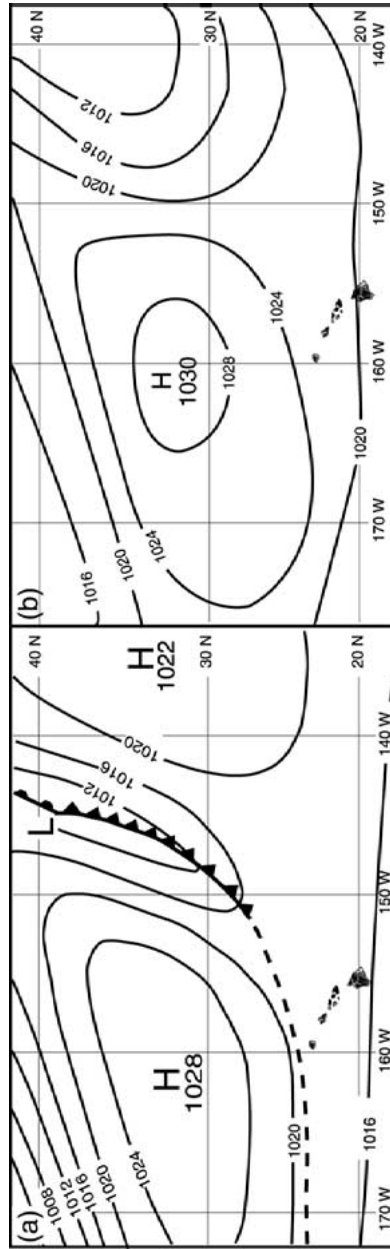


Figure 3. Sea-level pressure analyses (every 4 hPa) for (a) 26 January 2000 at 0000 UTC (*day one* 1400 HST) and (b) 27 January 2000 at 0000 UTC (*day two* 1400 HST). Heavy dashed line indicates location of weakening shearline.

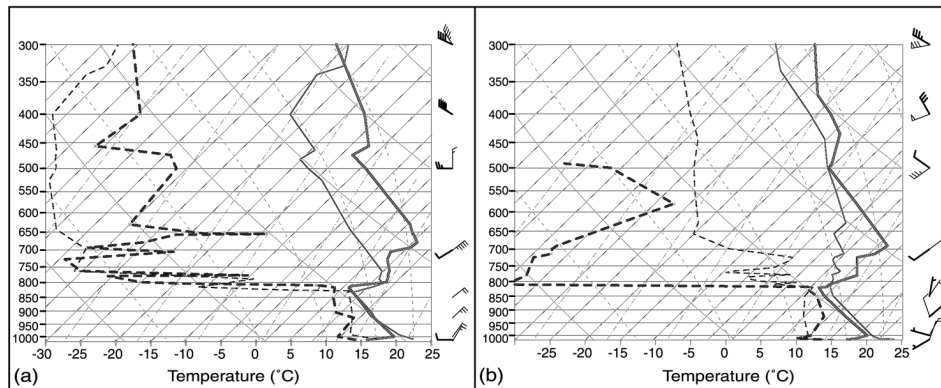


Figure 4. Skew-T log P diagrams showing temperature (solid) and dew point (dashed) soundings of temperature and dew point temperature on 25 January 2000 at 1200 UTC (*day one* 0200 HST) (thick lines) and 27 January 2000 at 0000 UTC (*day two* 1400 HST) (thin lines) at (a) Lihue and (b) Hilo.

time. In Hilo, the approaching shear line weakened the inversion layer from 3 °C to 1 °C, and the inversion base rose from 1810 to ~2480 m (725 hPa) (Figure 4b). At this time sun photometer measurements are concluding.

The presence of a strong and relatively low inversion layer was apparent during the commercial flight to the Island of Hawaii on day one, with the coasts of Maui and Hawaii barely visible through a thick blanket of vog, while the summits of Haleakala and Mauna Kea were quite clear (Figure 1). After landing in Keahole-Kona International Airport at 2130 UTC (0830 HST), conditions were cloud free, but there was a distinct volcanic haze surrounding the airport, and farther southward from the airport the haze became more distinct.

The morning of day two in Hilo, the sky was exceptionally clear, indicating subsidence was still quite strong. The observatories on the summit of Mauna Kea, located 16 km to the northwest, were clearly visible. These conditions allowed for excellent sun photometer measurements. However, solar heating during the morning resulted in the formation of cumulus clouds starting at 1900 UTC (0900 HST). Diurnal and orographic enhancement of the cumulus impacted the distribution of sun photometer measurements, discussed further in Section 5. During the two-day period, no rainfall was recorded in or near the areas under observation.

5. Results

The results are divided into four parts in this section (i) presentation of HY-SPLIT plume time series, (ii) comparison of HY-SPLIT graphical model output vs. satellite imagery, (iii) comparison of HY-SPLIT quantitative model output vs. waypoint observations, and (iv) presentation of aircraft observations.

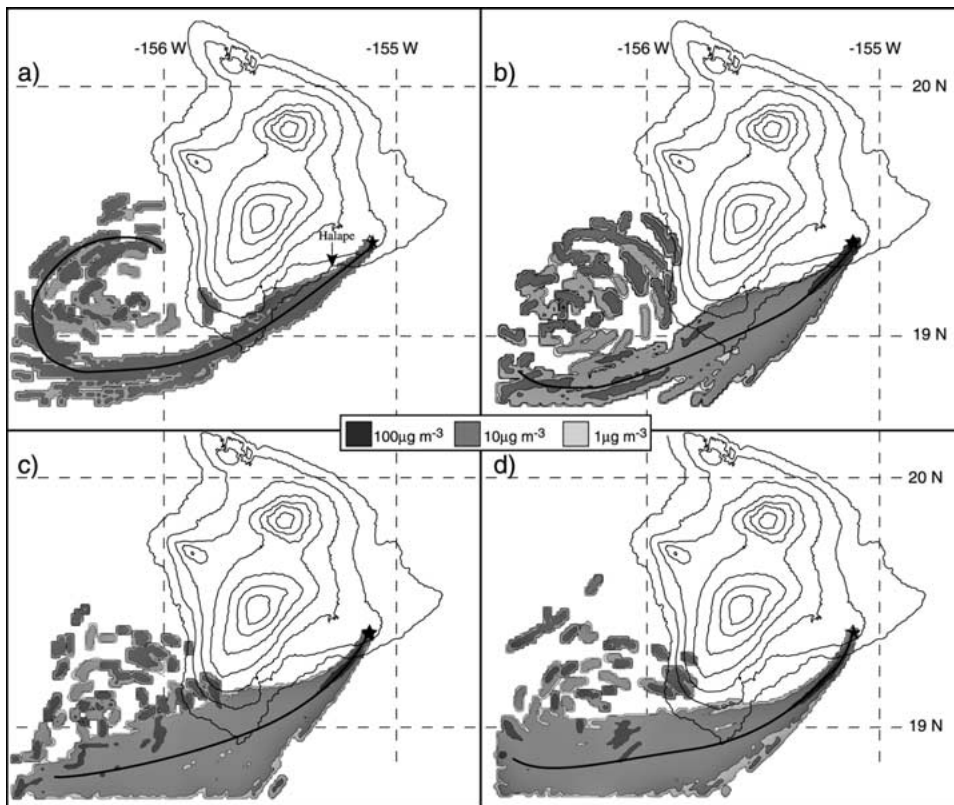


Figure 5. 3-D Particle HYSPLIT Model simulation of column average sulfate concentration from the surface to 2 km for 26 January 2000 at (a) 1800, (b) 2100, (c) 0000 and (d) 0300 hrs UTC. Black line indicates estimated plume centroid.

Aerosol concentration maps were created from HY-SPLIT 3-D particle model output to illustrate plume evolution (Figure 5). Because most of the observational data for comparison was gathered on day two, only day two's time series will be presented here. The initial release time for the modelled pollution depicted in these maps was 0100 UTC on 26 January to provide time for the vog to be advected to the Kona Coast.

The simulation results show skill in reproducing general shape of the plume evolution based upon the background synoptic conditions and orographic impact of the island. The plume experienced a south-westward motion as it was advected off the Halape coast, and the movement continued to the west-south-west where the plume traverses South Point. The plume continued with a predominately westward track (Figures 5b–d). The model consistently takes the maximum concentration of the plume over South Point. The slight directional shift of the plume off the Halape coast is in response to increasing wind speeds from a strengthening high-pressure system at this time (Figure 3). In Figures 5b and 5c the concentration

slightly decreases as a result of increased dispersion associated with the increased background flow. Plume eddies in the lee of the mountains are well captured. This dynamic effect aids in advecting aerosol into the south Kona coast (e.g., Figure 5c). The Kona coast experiences little sulfate before 1800 HST on day two, because of the spin up time necessary to advect realistic concentrations this far from the source, and the absence of background pollution in the model run. However, Figure 5 shows only a small area of the Kona coast impacted by aerosol over the time period of the simulation.

The satellite image for day two shows a narrow plume off the south-eastern coast of the Island of Hawaii, extending from the source to South Point, just missing the Halape area (Figure 6a). The satellite image depicts a thin, constrained plume near the source. There were also high levels of pollution along the Kona coast, supporting earlier visual observations. Inferences of aerosol concentration cannot be made over land from the satellite data since the algorithm used relies on derived ocean color. For comparison, Figure 6b shows the HY-SPLIT 3-D particle concentration valid at the time of the satellite image. The plume orientation, east-north-east to west-south-west, and the clear slot over Halape are in good agreement with satellite observations. However, the model's lack of enhanced pollution along the Kona coast disagrees with satellite observation.

Sun photometer measurements taken on day two under mostly clear conditions in the Hilo and Puna areas (waypoints 1, 3 and 4, Figure 7a) are characteristic of background concentrations, averaging $1.57 \mu\text{g m}^{-3}$ (Figure 7b). As mentioned previously, this may be representative of background sea-salt aerosol. The measurement at waypoint 2 was taken downwind of the Hawaiian Electric Company's Puna power plant, an SO_2 emitter, which may explain the increase in aerosol seen at this location. As expected, model values were several orders of magnitude smaller in this area upwind of the model source.

Cumulus buildup occurred on the uphill journey southward toward Hawaii Volcanoes National Park, because of orographic enhancement, and no measurement was possible in the park until about 100 m west of the entrance. The clouds began to break up on approach to South Point where measurements were again possible. Sun photometer-derived values remain low from waypoint 5 to 7 (Figure 7). These small values observed south-west of the vent can be explained by a residual drainage flow down the slope of Mauna Loa, shifting the aerosol plume and residual aerosol just offshore of South Point during the mid morning (1000 HST). Visual observations made at waypoint 7 indicated an aerosol haze to the south at this time. The model placed the greatest aerosol concentration over waypoints 6 and 7. It is suggested that the model plume is slightly misplaced northward relative to the observed plume for this time period, because of a lack of a diurnal land breeze in the MSM wind field, a point that will be returned to in the discussion section.

Satellite data and visual observations indicate that the plume axis shifted northward during day two as the sea-breeze circulation and the approach of the shear line increased the southerly component in flow over the South Point area. As a result,

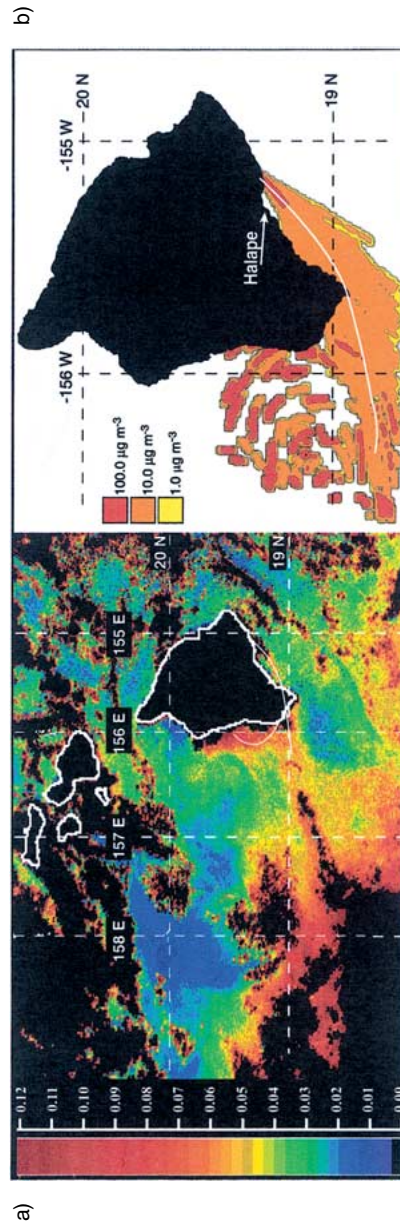


Figure 6. (a) SeaWiifs image that has been processed for aerosol optical depth valid at 2217 UTC (1217 HST) on 26 Jan 2000. (b) Modelled one-hr column averaged concentration ($\mu\text{g m}^{-3}$) for 2200 UTC on 26 January 2000. White solid lines represent estimated plume centroids.

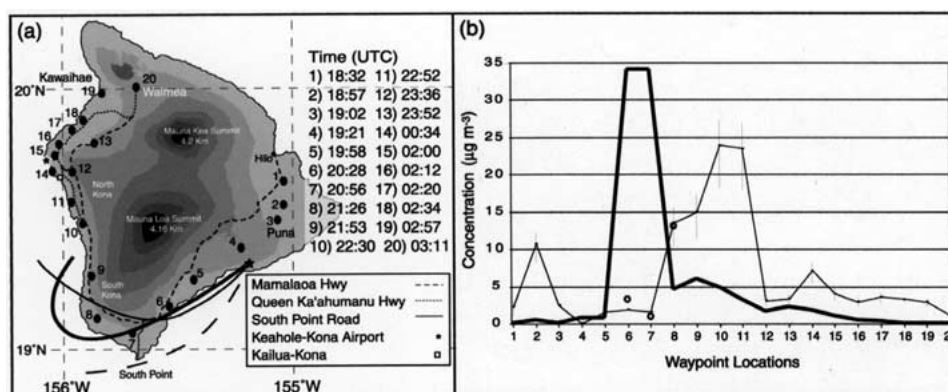


Figure 7. (a) 2000 January 26 waypoint locations and times. Estimated plume centroid location for sun photometer prior to 2100 UTC (long dash), post 2100 UTC (thin solid) and model (bold solid). (b) Part/Puff model (bold solid) vs. observed (thin solid) concentration values at waypoint locations with error bars varying relative humidity between 70–100% below 2000 metres. Circles represent 3-D particle model concentration values.

by noon the axis of the plume had approached waypoints 8 and 9, and the higher concentrations at these two sites may reflect proximity to the axis of maximum plume aerosol on day two (Figure 6).

The sun photometer measured the greatest aerosol burden over waypoints 10 and 11. It is suggested that these higher concentrations reflect aerosol accumulation during the extended period of stable conditions and light winds prior to the field experiment, rather than a plume-related maximum. The winds in this area tend to remain onshore or variable throughout the day in contrast to the rest of the Kona coastline, which usually experiences a component of offshore flow in the evening/late morning (Nash, 1992).

A decreasing aerosol content is observed from North Kona to Kawaihae. Concentrations drop off abruptly north of waypoint 11 and remain relatively constant at 2 to 3 $\mu\text{g m}^{-3}$ for the duration of the journey, with concentrations reducing gradually northward. The slight increase to 7.1 $\mu\text{g m}^{-3}$ at waypoint 14 may be due to its coastal location or proximity to contamination from upwind sources in Kailua-Kona, including a Hawaiian Electric Power Plant. The sun photometer and model output concentrations for waypoints 11–20 show similar trends, though the model consistently underestimates the observed values. However, the similarities between the 3-D particle model concentrations and the observed data are very good where comparisons are available.

Aircraft data document a distinct vog plume on day one (Figure 8). Sun photometer measurements were made through the open window of the Seneca starting at 0000 UTC on day one (1400 HST) along the Kona Coast. The pilot maintained a roughly south-south-west heading at an altitude of 100–200 m (Figure 8a). After passing through the bulk of the plume, he climbed to an elevation of approximately

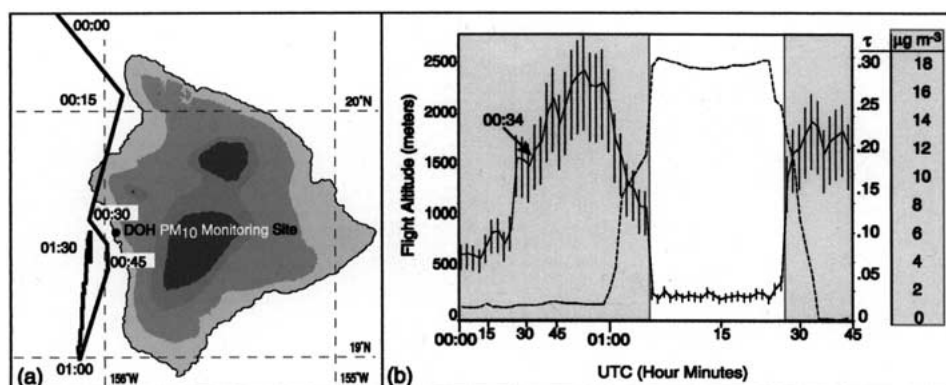


Figure 8. (a) Seneca aircraft flight pattern on 25 January 2000. (b) Sun photometer optical depths (τ) at 500 nm and sulfate calculations (valid in shaded areas only) with error bars varying relative humidity from 70–100% (solid) along with flight altitudes (dashed) retrieved via aircraft.

2400 m, well above the trade wind inversion (Porter et al., 2000). Figure 8b shows aerosol optical depths increasing from roughly 0.060–0.26 (no units) southward through the plume. As the aircraft passed the DOH PM10 monitoring site at 1434 HST, the aircraft-derived column sulfate concentration base value is $11.72 \mu\text{g m}^{-3}$ with error range from $8.93\text{--}13.4 \mu\text{g m}^{-3}$ (using σ_{sm} base-value and error ranges as described in Section 2). At the same time, the DOH PM10 measurement is $11.0 \mu\text{g m}^{-3}$, providing validation and confidence in derived sulfate calculations.

The aircraft data confirm that the vog is confined below the inversion level, since scattering optical depths drop from 0.274 to below 0.023, when climbing from 151 to 2452 m. It is important to note that conversion from optical depth to aerosol concentration was not valid at flight altitudes of 2000 m or greater as described in Equation (2), because the aerosol type is different. However, this large drop in optical depth above 2000 m is evidence that mixing of vog is inhibited by the inversion. Aircraft sun photometer data below the plume lasted for roughly 50 min in the northern Kona region just offshore (Figure 8a); the HY-SPLIT did not yet have sufficient spin-up time to reach this area, therefore quantitative comparisons were not possible. Since the background flow pattern did not change significantly between day one and day two, the increasing aerosol concentration southward of Kailua-Kona in the model data for day two is qualitatively consistent with the aircraft data on day one (i.e., Figures 7 and 8).

6. Conclusions and Discussion

Emissions from the Kilauea volcano pose significant environmental and health risks to the Hawaiian community. To mitigate these hazards, this study is aimed toward developing the ability to monitor and simulate the Kilauea volcanic plume. A field experiment was conducted on 25 and 26 January 2000 to collect data

to validate the modelling effort. The objective of the modelling component is to produce an accurate regional simulation of the concentration and dispersion of volcanic aerosol. The Hybrid Single-Particle Lagrangian Integrated Trajectory (HY-SPLIT) model was used for this purpose (Draxler and Hess, 1997, 1998). The wind fields and thermodynamic data from the non-hydrostatic Mesoscale Spectral Model (MSM) were used as required input for the HY-SPLIT model. The results of concentration and dispersion simulations over the Island of Hawaii were compared with data derived from aircraft-based measurements, ground-based measurements and satellite observations.

6.1. CONCLUSIONS

Aircraft data and visual observations confirm the importance of the trade wind inversion in trapping aerosols in the boundary layer, documented by the large drop in aerosol optical depth during an ascent through the plume.

The model produced plume characteristics include size, shape, orientation, and concentration gradients that are consistent with those observed in satellite imagery. The model successfully reproduced a well-constrained plume and clear slot over Halape on day two as seen in the satellite imagery. Both satellite and ground-based data suggest that the model performs best over the southern portion of the island and downwind over the ocean.

Comparison of the model concentrations and sun photometer observations suggests that the model is able to produce reasonable plume concentrations and spatial gradients downwind of the source. Prognoses of aerosol concentration degraded with time and distance northward along the Kona Coast. A low average aerosol concentration ($1.57 \mu\text{g m}^{-3}$) observed upwind of the vent during the field experiment reflects a relatively clean background concentration. Model aerosol concentrations upwind of the vent were even lower, because of the absence of upwind sources.

6.2. DISCUSSION

Given that this research is a first step toward simulation of the trajectory and dispersion of volcanic aerosol in the vicinity of Kilauea, the results can be viewed as promising. However, there clearly is room for additional work. Perhaps the greatest deficiency in the model was the underestimate of the aerosol concentrations moving northward along the Kona Coast. This deficiency may be due to one or a combination of several factors: (i) The absence of aerosol in the model initial condition, (ii) the absence of local sources of pollution along the leeward coast, or (iii) a lack of diurnal circulation in the model wind field.

Model data show that the vog plume is advected by the mesoscale flow from its origin, westward past South Point where vog accumulates and becomes enveloped in the lee eddy. Aircraft data suggest that even in this area, model concentrations were under-forecast. A reasonable explanation for lower model concentrations in

the lee of the island is that for an extended period of time, light and variable winds at the source caused aerosol to accumulate, raising background concentrations prior to the field experiment. On transit flights to the Island of Hawaii for the field experiment and during research aircraft flights, participants observed an unusual reduction in visibility due to the vog, supporting this suggestion. These background concentrations were not included in this study. Future modelling efforts will include estimates of background concentrations derived from satellite data in the initial condition of the model.

Since the performance of the HY-SPLIT model depends on the accuracy of the output from the MSM, deficiencies in the MSM wind field are reflected in HY-SPLIT concentration output. A significant diurnal cycle in the wind field was observed during the field experiment, as a result of light synoptic-scale trade winds and differential surface heating. The onshore sea-breeze flow that results is a key mechanism for advecting aerosol onto the Kona coast from offshore. The absence of aerosol advection onto the leeward coast in the HY-SPLIT model can be traced to the MSM wind field (Figure 9). The observed data suggest a directional change from 70–280 degrees from midnight to noon respectively and wind speed ranges from 0–5 m s⁻¹ during the day, whereas the MSM predicted wind on the leeward side experiences no meaningful speed fluctuation or directional reversal. Moreover, nocturnal downslope winds, also poorly represented in the MSM output, may have caused a shift in the location of the model plume along the southeast side of the island relative to the observed position.

In the research presented here, model temperature and humidity profiles were forced to reflect the observed inversion strength, resulting in a better simulation of aerosol dispersion. In an operational configuration the strength and evolution of the inversion needs to be accurately simulated by the mesoscale NWP model. It is anticipated that use of higher resolution output, particularly in the vertical, will improve this aspect of the modelling effort in future. Hawaii's complex terrain, mesoscale organization of weather systems, and lack of observational data over the central Pacific create substantial challenges for mesoscale models like the MSM. These, along with the issue of diurnal circulations, are subjects of active research, and progress in mesoscale NWP modelling will benefit the ongoing effort to simulate vog dispersion. Work is currently in progress to utilize output from enhanced resolution MM5* simulations in an effort to improve this aspect of the prediction system.

It has been suggested that the under-forecast of leeward aerosol concentration may be due in part to an overestimate of the explicit deposition over ocean in the model. The HYSPLIT model assumes that concentrations are uniform throughout the layer, whereas observed aerosols tend to concentrate nearer the top of the boundary layer. Therefore, in the mean, the model aerosol is nearer the surface where it can more quickly be lost to deposition. However, for the size distribution

* NCAR/Penn State University Mesoscale Model Version 5.

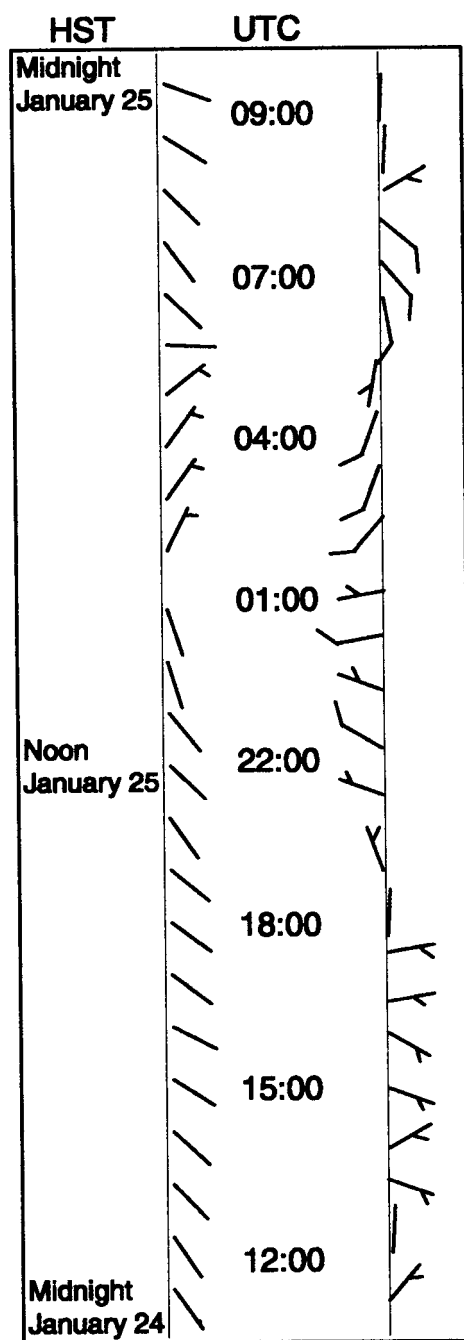


Figure 9. MSM (left) and observed (right) surface winds (m s^{-1}) at Keahole-Kona Airport on 25 January 2000 from 0000–2300 HST.

of the aerosol, the average deposition velocity in the model is only 1 mm s^{-1} . Over a 2-km deep boundary layer, in the absence of vertical mixing, it would require approximately 20 days for the aerosol to leave the column. Therefore, this is a negligible factor to the under-forecast.

In this study all the SO_2 was converted to SO_4 at the source to reduce computational requirements and because of uncertainties in a relatively fast conversion rate. The conversion rate is dependent on a number of factors including ambient water-vapour pressure, lava and land surface temperature, vent location and structure, volcanic activity, incoming solar radiation/cloud cover, and wind speed. Recent ground-based measurements have been made to investigate the SO_2 to sulfate conversion rate. Work is in progress to implement a dynamic conversion process in the model to improve the accuracy of predictions, particularly nearer the vent, and to include SO_2 concentrations as output.

Wet deposition was not a factor in this study because of dry weather conditions. To the extent that wet deposition represents a significant removal process it should to be included in the development of the ideal prognostic tool. Prediction of convective precipitation in complex terrain by mesoscale NWP models remains a great challenge. Fortunately, the stagnant conditions most conducive to significant pollution episodes tend to be dry.

During this study, one source location, the Pu'u O'o vent was used. Although the Pu'u O'o vent is the most important source during the time frame under study, the locations and rates of SO_2 emission change with time. In the ideal prediction system, all pertinent sources and their rates would be accurately represented. High-resolution satellite, local COSPEC, and mobile LIDAR measurements could be used in combination to better define the source distribution. Anthropogenic sources, though contributing significantly less in magnitude, could also be added.

Several observational experiments are planned during the next several years on the Island of Hawaii to collect data for analysis and model validation. Future model development and sensitivity studies are planned utilizing these data sets. The goal of this extended effort is the development of an increasingly accurate prognostic tool to help mitigate the negative impacts of Kilauea's volcanic emissions on the environment and on society.

Acknowledgments

The authors would like to thank Jeff Sutton and Tamar Elias at USGS Volcanoes National Park for their support and cooperation in this effort. They would also like to acknowledge the assistance of Derek Funayama and Bruce Anderson in the MSM modelling effort. We also appreciate the use of computing resources and staff expertise at the Maui High Performance Computing Center in Kihei, Maui. This research is supported by NASA under grant NAG5-9580. The NWP effort was partially supported by NASA/Scripps grant NAG5-8780. This is School of Ocean and Earth Science and Technology contribution 6092.

References

- Charlson, R. J., Langner, J., Rodhe, H., Leovy, C. B., and Warren, S. G.: 1991, 'Perturbation of the Northern Hemispheric Radiative Balance by Backscattering from Anthropogenic Sulfate Aerosols', *Tellus* **43AB**, 152–163.
- Clarke, A. D. and Porter, J.: 1991, 'Volcanic Haze: Physiochemistry and Transport', in *Vog and Laze Seminar*, Hilo, HI, Center for the Study of Active Volcanoes (unpag.).
- Draxler, R. R. and Hess, G. D.: 1997, *Description of the HY-SPLIT_4 Modelling System*, NOAA Tech. Memo. ERL-ARL224, December, 24 pp. (NTIS, 5285 Port Royal Road, Springfield, VA 22161.)
- Draxler, R. R. and Hess, G. D.: 1998, 'An Overview of the HY-SPLIT_4 Modelling System for Trajectories, Dispersion and Deposition', *Aust. Meteorol. Mag.* **47**, 295–308.
- Draxler, R. R., McQueen, J. T., and Stunder, B. J. B.: 1994, 'An Evaluation of Air Pollutant Exposures Due to the 1991 Kuwait Oil Fires Using a Lagrangian Model', *Atmos. Environ.* **28**, 2197–2210.
- Elias, T.: 1992, 'The Effect of Volcanic Emissions on Ambient Air Quality in Hawaii Volcanoes National Park', in *Abstracts*, Hilo, HI, University of Hawaii at Hilo, Center for the Study of Active Volcanoes (unpag.).
- Elias, T., Sutton, A. J., Stokes, J. B., and Casadevall, T. J.: 1998, *Sulfur Dioxide Emission Rates of Kilauea Volcano, Hawaii, 1979–1997*, USGS open-file report 98-462.
- Feng, J. and Chen, Y.-L.: 1998, 'Evolution of Katabatic Flow on the Island of Hawaii on 10 August 1990', *Mon. Wea. Rev.* **126**, 2185–2199.
- Gerlach, T. M.: 1993, 'Oxygen Buffering of Kilauea Volcanic Gases and the Oxygen Fugacity of Kilauea Basalt', *Geochim. Cosmochim. Acta* **57**, 796–814.
- Gerlach, T. M. and Casadevall, T. J.: 1986, 'Evaluation of Gas Data from High-Temperature Fumaroles at Mount St. Helens, 1980-1982', *J. Volc. Geotherm. Res.* **28**, 107–140.
- Giambelluca, T. W., Nullet, D., and Schroeder, T. A.: 1986, 'Average Annual and Monthly Rainfall', in *Rainfall Atlas of Hawaii, State of Hawaii*, Department of Land and Natural Resources.
- Gordon, H. R.: 1997, 'Atmospheric Correction of Ocean Color Imagery in the Earth Observing System Era', *J. Geophys. Res.* **102D**, 17081–17106.
- Grinding, C. M.: 1992, *Temporal Variability of the Trade Wind Inversion: Measured with a Boundary Layer Vertical Profiler*, Master's Thesis, University of Hawaii. (Available from Department of Meteorology, 2525 Correa Road, Honolulu, Hawaii, 96822.)
- Harris, A. J. and Thornber, C. R.: 1999, 'Complex Effusive Events at Kilauea as Documented by the GOES Satellite and Remote video Cameras', *Bull. Volcan.* **61**, 382–395.
- Hoppel, W. A., Fitzgerald, J. W., Frick, G. M., and Larson, R. E.: 1987, *Preliminary Investigation of the Role that DMS and Cloud Cycles Play in the Formation of the Aerosol Size Distribution*, NRL Report 9032.
- Hurley, P. J.: 1994, 'PARTPUFF – A Lagrangian Particle-Puff Approach for Plume Dispersion Modelling Applications', *J. Appl. Meteorol.* **33**, 285–294.
- Juang, H.-M. H.: 1992, 'A Spectral Fully Compressible Nonhydrostatic Mesoscale Model in Hydrostatic Sigma Coordinates: Formulation and Preliminary Results', *Meteorol. Atmos. Phys.* **50**, 75–88.
- Juang, H.-M. H.: 2000, 'The NCEP Mesoscale Spectral Model: A Revised Version of the Non-hydrostatic Regional Spectral Model', *Mon. Wea. Rev.* **128**, 2329–2362.
- Juang, H.-M. H. and Kanamitsu, M.: 1994, 'The NMC Nested Regional Spectral Model', *Mon. Wea. Rev.* **122**, 3–26.
- Juang, H.-M. H., Hong, S.-Y., and Kanamitsu, M.: 1997, 'The NCEP Regional Spectral Model: An Update', *Bull. Amer. Meteorol. Soc.* **78**, 2125–2143.
- Kidder, S. Q. and Vonder Haar, T. H.: 1995, 'Radiative Transfer', in *Satellite Meteorology: An Introduction*, Academic Press, San Diego, pp. 47–86.

- Kleinman, M.: 1995, 'Health Effects of Inhaled Particles and Acid Sulfate Aerosols', in *Vog Symposium*, Honolulu, HI, Department of Health (unpag.).
- Mannino, D. M., Ruben, S. M., and Holschuh, F. C.: 1995, 'Weekly Variability of Emergency Room Visits for Asthma in Hilo, Hawaii, 1981–1991', in *Vog Symposium*, Honolulu, HI, Department of Health (unpag.).
- Morrow, J. W.: 1991, 'The Atmospheric Fate of Sulfur Gases from Kilauea Volcano', in *Vog and Laze Seminar*, Hilo, HI, Center for the Study of Active Volcanoes (unpag.).
- Morys, M. F., Mims III, F. M., and Anderson, S. E.: 1996, 'Design, Calibration and Performance of MICROTOPS II Hand-Held Ozonometer', in *12th International Symposium on Photobiology*, Vienna, Austria, International Congress on Photobiology. (Available online at <http://www.solar.com/ftp/papers/mtops.pdf>.)
- Nash, A. J.: 1992, *Diurnal Variation in Wind Direction and Speeds on Hawaii Island*, in B. Bays (ed.), *SOEST Report 1991–1992*, School of Ocean and Earth Science and Technology, 2525 Correa Road, University of Hawaii, Honolulu, HI, 96822.
- Palmer, K. F. and Williams, D.: 1975, 'Optical Constants of Sulfuric Acid: Application to the Clouds of Venus?', *Appl. Opt.* **14**, 208–219.
- Porter, J. N. and Clarke, A. D.: 1997, 'Aerosol Size Distribution Models Based on *in situ* Measurements', *J. Geophys. Res.* **102**(D5), 6035–6045.
- Porter, J. N., Clarke, A., and Lienert, B.: 2000, 'Aircraft/Surface Derived Aerosol Optical Properties near Hawaii for Satellite Validation', in *Proceedings of the SPIE Remote Sensing of the Atmosphere, Environment and Space*, Sendai, Japan, ISBN 0-7803-6362-0, 8 pp.
- Porter, J. N., Miller, M., Pietras, C., and Motell, C.: 2001, 'Ship-Based Sunphotometer Measurements Using Microtops Sun Photometers', *J. Atmos. Oceanic Tech.* **18**, 765–774.
- Pruppacher, H. R. and Klett, J. D.: 1978, *Microphysics of Clouds and Precipitation*, D. Reidel Publishing Company, Dordrecht, Norwell, MS, 714 pp.
- Realmuto, V. J., Sutton, A. J., and Elias, T.: 1997, 'Multispectral Thermal Infrared Mapping of Sulfur Dioxide Plumes: A Case Study from the East Rift Zone of Kilauea Volcano, Hawaii', *J. Geophys. Res.* **102**(B7), 15,057–15,072.
- Ruben, S. M., Mannini, D. M., Holschuh, F. C., Holschuh, T. C., Wilson, M. D., and Holschuh, T.: 1995, 'Emergency Room Visits for Asthma and Chronic Obstructive Pulmonary Disease on the Island of Hawaii, 1981–1991', in *Vog Symposium*, Honolulu, HI, Department of Health (unpag.).
- State of Hawaii, Department of Health, Env. Mgmt. Div. Safe Drinking Water Branch, 1989: Extended Abstract, in *4th International Conference on Water Cistern Systems*, Makati Metro, Philippines.
- Sutton, J. and Elias, T.: 1993, 'Volcanic Gases Create Air Pollution on the Island of Hawaii', *Earthquakes Volcanoes* **24**(4), 178–196.
- Sutton, J. and Elias, T.: 1996, 'Volcanic Emissions from Kilauea and their Effect on Air Quality', *Hawaii Med. J.* **55**(3), 46 (Abstract).
- Sutton, J. and Elias, T.: 1997, 'Volcanic Gases, Vog and Laze: What They Are, Where They Come From, and What They Do?', in *Abstracts*, Hilo, HI, University of Hawaii at Hilo, Center for the Study of Active Volcanoes, p. 1.
- Symonds, R. B., Rose, W. I., Bluth, G. J. S., and Gerlach, T. M.: 1994, 'Volcanic-Gas Studies: Methods, Results and Applications', *Rev. Mineral.* **30**, 1–60.
- USGS Hawaiian Volcano Observatory: cited 2000, 'Archive of Previous Eruption Updates' (available on-line from http://hvo.wr.usgs.gov/kilauea/update/archive/2000/Feb/20000229_flowmap_800.jpg)
- Worth, R. M.: 1995, 'Respiratory Impacts Associated with Chronic VOG Exposure on the Island of Hawaii', in *Vog Symposium*, Honolulu, HI, Department of Health (unpag.).
- Zhang, L., Gong, S., Padro, J., and Barrie, L.: 2001, 'A Size-Segregated Particle Dry Deposition Scheme for an Atmospheric Aerosol Module', *Atmos. Env.* **35**, 549–560.